Contents

%newpage

Chapter 1

Verification and Validation

Computer simulations are in many engineering applications a cost-efficient way for conducting design and performance optimalization of physical problems. However, thrusting blindly numbers generated from a computer code can prove to be naive. It doesn't take a lot of coding experience before one realizes the many things that can brake down and produce unwanted or unexpected results. Therefore, *credability* of computational results are essential, meaning the simulation is worthy of belief or confidence [24]. *Verification and validation* (V&V) is the main approach for assessing and the reliability of computational simulations [36]. A thorough discussion of (V&V) concepts and terminology during the last century can be found in [24]. In this thesis, the definitions provided by the *American Society of Mechanical Engineers guide for Verification and Validation in Computational Solid Mechanics* [33] are followed.

Definition 1.1. Verification: The process of determining that a computational model accurately represents the underlying mathematical model and its solution.

Definition 1.2. Validation: The process of determining the degree to which a model is an accurate representation of the real world from the perspective of the intended uses of the model.

Simplified *verification* considers if one solves the equations right, while *validation* is checking if one solves the right equations for the given problem [30].
To test a computational code for all possible parameters, conditions and applications are simply too time consuming. Verification and validation are therefore ongoing processes, with no clear boundary of completeness unless additional requirements are specified [30]. The goal of this chapter is to verify our implementations using the method of manufactured solution (MMS), addressing validation in a later chapter.

1.1 Verification of Code

Within scientific computing a mathematical model is often the baseline for simulations of a particular problem of interest. For scientists exploring physical phenomena, the mathematical model is often on the form of systems of partial differential equations (PDE´s). A computer program therefore must evaluate mathematical

identities such a differential operators and functions in order to produce accurate solutions of the governing PDE´s. Through verification of code, the ultimate goal is to ensure a computer program truly represents the mathematical model. To accumulate sufficient evidence that a mathematical model is solved correctly by a computer code, it must excel within predefined criteria. If the acceptance criterion is not satisfied, a coding mistake is suspected. Should the code pass the preset criteria, the code is considered verified. Of the different classes of test found in [30], *Order-of-accuracy* (OAA) is regarded as the most rigorous acceptance criterion for verification [32], [30], [5]. In addition to error estimation and convergence of the numerical solution, the method ensure the discretization error E is reduced in coordinance with the *formal order of accuracy* expected from the numerical scheme. The formal order of accuracy is defined to be the theoretical rate at which the truncation error of a numerical scheme is expected to reduce. The *observed order of accuracy* is the actual rate produced by our code. The order of convergence is calculated xAssuming a PDE of space and time, order-of-accuracy tests are conducted separaty of
By monitoring the dicretization error E by spatial and temporal refinements, one assumes the asymptotic behavior,

$$E = E_x + E_t = u_e - u_h = C\Delta t^p + D\Delta x^l$$

where C is a constant, h represents the spatial or temporal resolution, and p is the convergence rate of the numerical scheme. For order of convergence tests, the code is assumed to be verified if the discretization error is proportional to h^p.

1.1.1 Method of manufactured solution

The basis of a convergence test is how to find an exact/reference solution, in order to compute the discretization error E. However solutions of PDE´s are limited, and often simplifications of the original problem are needed to produce analytically solutions. *The method of manufactured solutions* provides a simple yet robust way of making analytic solutions for PDE´s. Let a partial differential equation of interest be on the form

$$\mathbf{L}(\mathbf{u}) = \mathbf{f}$$

Here $\mathbf{L}$ is a differential operator, $\mathbf{u}$ is variable the of interest, and $\mathbf{f}$ is some sourceterm. In the method of manufactured solution one first manufactures a solution $\mathbf{u}$ for the given problem. In general, the choice of $\mathbf{u}$ will not satisfy the governing equations, producing a sourceterm $\mathbf{f}$ after differentiation by $\mathbf{L}$. The produced source term will cancel any imbalance formed by the manufactured solution $\mathbf{u}$ of the original problem. Therefore, the manufactured solution can be constructed without any physical reasoning, proving code verificaion as a purely a mathematical exercise were our only interest is to verify the solution [29]. If the MMS is not chosen properly the test will not work, therfore some guidelines for rigirous verification have been proposed in [5, 32, 29].

- The manufactured solution (MS), should be composed of smooth analytic functions such as exponential, trigonometric, or polynomials.
- The MS should should have sufficient number of derivatives, exercising all terms and derivatives of the PDE´s.

To deeply verify the robustness of the method of manufactured solution, a report regarding code verification by MMS for CFD was published by Salari and Knupp [32]. This thorough work applied the method for both compressible and incompressible time-dependent Navier-Stokes equation. To prove its robustness the authors deliberate implemented code errors in a verified Navier-Stokes solver by MMS presented in the report. In total 21 blind testcases where implemented, where different approaches of verification frameworks were tested. Of these, 10 coding mistakes that reduces the observed order-of-accuracy was implemented. Here the method of manufactured solution captured all coding mistakes, except one. This mistake would, accordingly to the co-author , been captured if his guidelines for conducting MMS had been followed. In general, computing the source term f can be quite challenging and error prone. Therefore, symbolic computation of the sourceterm is advantigous to overcome mistakes which can easily occur when calulating by hand. For construction of the sourceterm **f**, the Unified Form Language (UFL) [**?**] provided in FEniCS Project will be used.

1.1.2 Verification of the fluid-structure interaction solver by MMS

In general the MMS does not need to match any physical capabilities. However, when considering multiphysics problems, such as FSI, the equations has to meet the mathematical criteria of the interface.

1. Kinematic boundary condition $\hat{\mathbf{v}}_s = \hat{\mathbf{v}}_f$, enforced strongly by a continious velocity field in the fluid and solid domain.
2. Dynamic boundary condition $\sigma_s \cdot \mathbf{n} = \sigma_f \cdot \mathbf{n}$, enforced weakly by omitting the boundary integrals from the weak formulation in problem.

The choice of a MMS is therefore not trivial, as it must fulfill condition 1 and 2, in addition to the divergence-free condition in the fluid, and avoiding cancellation of the ALE-convective term $/pder\hat{T}_f t$. The struggle is reflected of the abscence of research, regarding MMS for coupled FSI solvers in the litterature. The challenge are often disregarded, such as [34], where the verification process is conducted on the fluid and structure solver separately. Instead, the correctness of the coupling is evaluated by the code validation. The approach clearly ease the process, assuming verification of each codeblock is "sufficient" to declare the code verified. It must be stressed that solving each problem individually is not true verification, in reference to a monolithic approach where the problems are solved at the same time.
The construction of a MMS for a monolithic FSI problem is therefore out of the scope of this thesis. Conducting verification on the fluid and structure separatly is not , but considered "good enough" to show the mathematical model is discretized accuratly.

1.2 Validation of the one-step θ scheme

Through *verification*, one can assure that a scientific code implements a mathematical model correctly. However, correctness is unnecessary if the model fails to serve as an accurate representation of the physical problem of interest. By definition 1.2, *Validation* is the act of demonstrating that a mathematical model is applicable for its intended use with a certain degree of accuracy. That is, a mathematical model is validated if it meets some predefined criteria within a specific context. Validation is therefore not intended to portray the model as an absolute truth, nor the best model available [31]. In computational science, validation is conducted by comparing numerical results against existing experimental data. The design of validation experiments vary by the motivation of the of their creators, where validated experiments for computational science can be divided into three groups[36] (1)To improve fundamental understanding of a physical process, (2) Discovery or enhancement of mathematical models of well known physical processes, (3) to conclude the reliability and performance of systems. The assessment of comparison between numerical results and experimental data,makes *validation* assess a wide range of issuses [36] . Is the experiment relevant, and conducted correctly in accordinance with prescribed parameters? What about the measurement uncertainty of reference experimental data? These issues must be addressed in order to raise sufficient confidence that the mathematical model is credible for its intended use.

Validation of CFSI is demanding due to the number of building blocks composing the full problem. For *interface-tracking* methods such as the ALE-method, validation is not only related to the physical aspcets of the model. Even if the fluid and strucutre models excel well within predefined criteria, the non-physical nature of mesh moving models have proven to affect the numerical solution [45]. At first glance, this effect is surprising as mesh moving models simply describe the evolution of fluid mesh cells from the moving interface. However, each mesh model distributes the fluid cells differently, which in turn may have an important effect when conducting mathematical operations such as gradients.

The numerical benchmark presented in [15] has been chosen for validation of the *One-step θ* scheme from chapter 3. The benchmark has been widely accepted throughout the fluid-structure interaction community as a rigid validation benchmark [45, 47, 40, 11]. This is mainly due to the diversity of tests included, challenging all the main components of a fluid-structure interaction scheme.
The computational domain is based on the *von Kármán vortex street* [43], where a cylinder is intentionally placed off center in a pipe. In [15], an elastic flag is placed behind the cylinder, see Figure 4.1

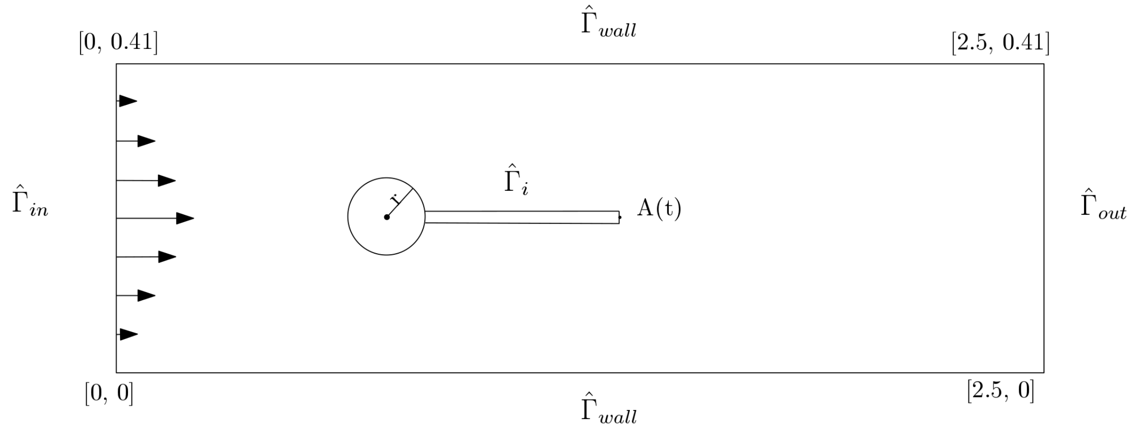

Figure 1.1: Computational domain of the validation benchmark

The benchmark is divided into three main test environments. In the first environment the fluid solver is tested for a series of different flow profiles. The second environment considers the structure solver, regarding bending of the elastic flag. And the final environment concerns validation the full fluid-structure interaction problem. The test environments are further divided into three different problems with increasing difficulty, posing different challenges to the implementation.

Several quantites for comparion are presented in [15] for validation purposes.

- The position (x,y) of point A(t) as the elastic flag undergoes deformation.
- Drag and lift forces exerted on of the whole interior geometry in contact with the fluid, consisting of the rigid circle and the elastic beam.

$$(F_D, F_L) = \int_{\Gamma} \sigma \cdot \mathbf{n} dS$$

All environments pose both steady state and periodic solutions. For the steady state solutions, the quantity of interest will be calculated for the last time step. For the periodic solutions, the amplitude and mean values for the time dependent quantity are calculated from the last period of oscillations.The mean value and amplitude is given by,

$$\begin{aligned} \text{mean} &= \frac{1}{2}\text{max} + \text{min} \\ \text{amplitude} &= \frac{1}{2}\text{max - min} \end{aligned}$$

from the maximum and minimum value of the quantity of interest from the last period. In [15], all steady state solutions seems to be calulated by solving a steady state equation since time-step are only reported for the periodic solutions. In this thesis, all problems in [15] are calculated by time integration. The main motivation is based upon that any given numerical errors regarding time integration will be intercepted at an earlier stage for a simpler problem. Therefore, the choice of time step is chosen such that reasonable accuracy of the reference solution is attained.
In the following section, an overview of each environment together with numerical results will be presented. A formal discussion of the results are given at the end of each simulation environment. For each table, the error of the finest spatial and temporal refinement compared to the reference solution is reported jn [15], and the followup work.

1.2.1 Validation of fluid solver

The first test environment conserns the fluid solver for low Reynold-number regime. Two approaches for the validation are given in [15]. The first approach considers the setup as a fluid-structure interaction problem, by setting the elastic flag close to rigid by manipulation of the structure parameters. In the second approach, the flag is set fully rigid and considered a purely flow problem. By this proposal, no deformation of the fluid domain occurs, reducing the fluid variation formulation to its original form,

$$\begin{aligned} (\frac{\partial \hat{\mathbf{v}}_f}{\partial t},\ \hat{\boldsymbol{\psi}}^u)_{\hat{\Omega}_f} + \big((\hat{\mathbf{v}}_f \cdot \hat{\nabla})\hat{\mathbf{v}}_f,\ \hat{\boldsymbol{\psi}}^u\big)_{\hat{\Omega}_f} - \big(\hat{\sigma},\ \hat{\nabla}\hat{\boldsymbol{\psi}}^u\big)_{\hat{\Omega}_f} - \big(\rho_f \mathbf{f}_f,\ \hat{\boldsymbol{\psi}}^u\big)_{\hat{\Omega}_f} &= 0 \\ \big(\nabla \cdot \hat{\mathbf{v}}_f),\ \hat{\boldsymbol{\psi}}^p\big)_{\hat{\Omega}_f} &= 0 \end{aligned}$$

The latter approach is chosen for this thesis, as only the variational formulation for the fluid is tested and removes any influence of the structure and mesh extrapolation discretization. The validation of the fluid solver is divided into the three sub-cases; CFD1, CFD2, and CFD3. While CFD1 and CFD2 yields steady state solutions, CFD3 is a periodic solution.
A parabolic velocity profile on the form,

$$v_f(0, y) = 1.5U\frac{(H-y)y}{(\frac{H}{2})^2}$$

is set on the left channel inflow. H is the height of the channel, while the parameter U is set differently to each problem to induce different inlet flow profiles. At the right channel outflow, the pressure is set to $p = 0$. No-slip boundary conditions for the fluid are enforced on the channel walls, and on the inner geometry consisting of the circle and the elastic flag. The validation is based on the evaluation of drag and lift forces on the inner geometry for each sub-case. Each sub-case will be conducted on four different mesh, with increasing refinement. The following tables presents the numerical results for each sub-case.

Table 1.1: Benchmark environment

Fluid parameters			
parameter	CFD 1	CFD 2	CFD 3
$\rho^f [10^3 \frac{kg}{m^3}]$	1	1	1
$\nu^f [10^{-3} \frac{m^2}{s}]$	1	1	1
U	0.2	1	2
Re	20	100	200

Results

Table 1.2: CFD 1 Results

$\Delta t = 0.1$ $\theta = 1.0$			
nel	ndof	Drag	Lift
1438	6881	13.60	1.089
2899	13648	14.05	1.126
7501	34657	14.17	1.109
19365	88520	14.20	1.119
Reference		14.29	1.119
Error		0.006 %	0.00 %

Table 1.3: CFD-2

$\Delta t = 0.01$ $\theta = 1.0$			
nel	ndof	Drag	Lift
1438	6881 (P2-P1)	126.0	8.62
2899	13648 (P2-P1)	131.8	10.89
7501	34657 (P2-P1)	135.1	10.48
19365	88520(P2-P1)	135.7	10.55
Reference		136.7	10.53
Error		0.007 %	0.001 %

Table 1.4: CFD-3

$\Delta t = 0.01 \quad \theta = 0.5$			
nel	ndof	Drag	Lift
1438	6881 (P2-P1)	417.23 +/- 0.0217	-249.21 +/- 0.32
	16474 (P3-P2)	414.86 $\pm$ 5.6282	-7.458 $\pm$ 444.07
2899	13648 (P2-P1)	408.50 $\pm$ 4.3029	-19.731 $\pm$ 373.45
	32853 (P3-P2)	432.86 $\pm$ 5.5025	-9.686 $\pm$ 431.28
7501	34657 (P2-P1)	431.57 $\pm$ 5.2627	-12.497 $\pm$ 429.76
	83955 (P3-P2)	438.20 $\pm$ 5.5994	-11.595 $\pm$ 438.00
19365	88520 (P2-P1)	435.43 $\pm$ 5.4133	-11.545 $\pm$ 438.89
	215219 (P3-P2)	438.80 $\pm$ 5.6290	-11.158 $\pm$ 439.23
Reference		439.95 $\pm$ 5.6183	-11.893 $\pm$ 437.81
Error		0.002 % $\pm$ 0.001 %	0.061 % $\pm$ 0.003%
$\Delta t = 0.005 \quad \theta = 0.5$			
nel	ndof	Drag	Lift
1438	6881 (P2-P1)	417.24 $\pm$ 0.0084	-249.386 $\pm$ 0.1345
1438	16474 (P3-P2)	414.90 $\pm$ 5.7319	-8.467 $\pm$ 443.45
1438	13648 (P2-P1)	408.27 $\pm$ 4.0192	-18.981 $\pm$ 363.84
2899	32853 (P3-P2)	432.90 $\pm$ 5.5333	-11.382 $\pm$ 430.60
1438	34657 (P2-P1)	431.59 $\pm$5.2979	-13.644 $\pm$ 429.68
7501	83955 (P3-P2)	438.23 $\pm$ 5.6393	-12.917 $\pm$ 437.78
1438	88520 (P2-P1)	435.46 $\pm$ 5.4579	-13.190 $\pm$ 438.05
19365	215219 (P3-P2)	438.84 $\pm$ 5.6576	-12.786 $\pm$ 438.36
Reference		439.95 $\pm$ 5.6183	-11.893 $\pm$ 437.81
Error		0.002 % $\pm$ 0.006 %	0.075 % $\pm$ 0.001%

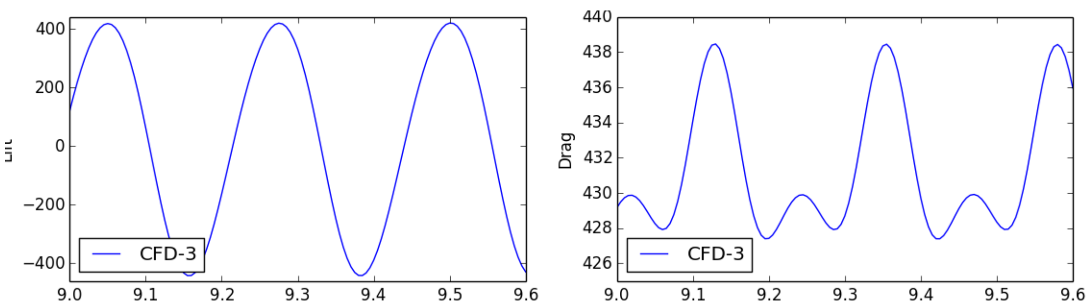

Figure 1.2: CFD-3, lift and drag forces at time t = [9, 9.6]

Discussion of results

The numerical results for CFD1, CFD2 and CFD3 are all within reasonable range of the reference solutions presented in [15]. For CFD1 and CFD2, the choice of P2-P1 elements together with a fully implicit schene $\theta = 1$ gained sufficient accuracy in

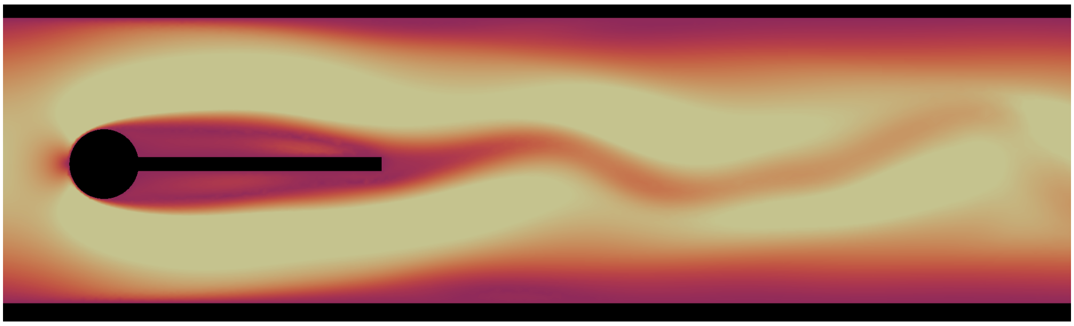

Figure 1.3: CFD-3, flow visualization of velocity time t = 9s

comparison with the reference solution. The second order cranc-nicholoson scheme $\theta = 0.5$ was investigated for CFD1 and CFD2, however only improving the results of order 10^{-6} for both lift and drag. For the periodic problem CFD-3, the choice of P2-P1 elements with a fully implicit time-stepping scheme proved unsufficient for capturing the expected periodic solution. By cranc-nicolson time-stepping scheme $\theta = 0.5$, the periodic solution was attained. Since the choice of finite-elemt pair is not reported in the original work, both P3-P2 and P2-P1 element pairs for fluid and pressure respectively was compared in combination with spatial mesh refinement. From Table 1.4, the choice P3-P2 element pair is eminent to achieve reasonable results for the first and second mesh regardless of timestep. However, the third and fourth mesh shows close resemblance with the reference solution. On this basis, the choice of P2-P1 element pair is sufficient for the evaluation of drag and lift on the inner geometry with increasing mesh resolution.

1.2.2 Validation of solid solver

Table 1.5: CSM validation environment

Fluid parameters			
parameter	CSM 1	CSM 2	CSM 3
$\rho^s[10^3 \frac{kg}{m^3}]$	1	1	1
ν^s	0.4	0.4	0.4
$\mu^s[10^6]$	0.5	2.0	0.5
$g\frac{m}{s^2}]$	2.0	2.0	2.0

The validation of the solid solver is conducted on a rectangular domain, representing the elastic structure behind the circle in Figure ?. The structure is submitted to a gravitational for $\mathbf{g} = (0, g)$, while beeing fixed to a fictional wall on the left side of the domain. The validation of the solid solver is based on comparison of the deflection of point $A(t) = [A_x(t), A_y(t)]$, conducted on three refined mesh, where the number of finite elements are chosen in close resemblance with the original work in [15]. A simple investigation of different finite-element pairs, suggest that P3-P3 elements where used for making the reference solution. In this study, lower order finite-element pair was included by the motivation of shorter simulation time while retaining solution accuracy. While computational time is not a major concern for the solid solver, the study is important for potentially reducing the computational time for the final validation environment.

Table 1.6: CSM 1 Results

$\Delta t = 0.1 \;\; \theta = 1.0$			
nel	ndof	ux of A [x 10^3]	uy of A [x 10^3]
319	832 P1-P1	-5.278	-56.6
	2936 P2-P2	-7.056	-65.4
	6316 P3-P3	-7.064	-65.5
1365	3140 P1-P1	-6.385	-62.2
	11736 P2-P2	-7.075	-65.5
	25792 P3-P3	-7.083	-65.5
5143	11084 P1-P1	-6.905	-64.7
	42736 P2-P2	-7.083	-65.4
	94960 P3-P3	-7.085	-65.5
Reference		-7.187	-66.1
Error		1.41 %	0.8 %

Discussion of results

The results for sub-problems CSM-1 and CSM-2 each coincide with the reference solution. The study of lower-grade elements proved successful for both problems, justifying accurate results can be achieved for polynomials grade 1 and 2 for all mesh refinements. This observation is further justified in the CSM-3 results. In

Table 1.7: CSM 2 Results

$\Delta t = 0.05$ $\theta = 1.0$			
nel	ndof	ux of A [x 10^3]	uy of A [x 10^3]
319	832 P1-P1	-0.3401	-14.43
	2936 P2-P2	-0.460	-16.78
	6316 P3-P3	-0.461	-16.79
1365	3140 P1-P1	-0.414	-15.93
	11736 P2-P2	-0.461	-16.81
	25792 P3-P3	-0.461	-16.82
5143	11084 P1-P1	-0.449	-16.60
	42736 P2-P2	-0.461	-16.82
	94960 P3-P3	-0.462	-16.82
Reference		-0.469	-16.97
Error		1.49%	0.88 %

Table 1.8: CSM 3 Results

$\Delta t = 0.02$ $\theta = 0.5$			
nel	ndof	ux of A [x 10^3]	uy of A [x 10^3]
319	832 P1-P1	-10.790 +/- 10.797	-55.184 +/- 56.682
	2936 P2-P2	-14.380 +/- 14.387	-63.198 +/- 65.147
	6316 P3-P3	-14.409 +/- 14.417	-63.288 +/- 65.225
1365	3140 P1-P1	-13.032 +/- 13.041	-60.446 +/- 62.075
	11736 P2-P2	-14.407 +/- 14.416	-63.283 +/- 65.220
	25792 P3-P3	-14.412 +/- 14.421	-63.310 +/- 65.246
5143	11084 P1-P1	-14.059 +/- 14.071	-62.591 +/- 64.473
	42736 P2-P2	-14.412 +/- 14.421	-63.313 +/- 65.249
	94960 P3-P3	-14.416 +/- 14.425	-63.328 +/- 65.263
Reference		-14.305 +- -14.305	-63.607 +- 65.160
Error		%	%

$\Delta t = 0.01$ $\theta = 0.5$			
nel	ndof	ux of A [x 10^3]	uy of A [x 10^3]
319	832 P1-P1	-10.835 +/- 10.836	-55.197 +/- 56.845
	2936 P2-P2	-14.390 +/- 14.392	-63.303 +/- 65.149
	6316 P3-P3	-14.432 +/- 14.435	-63.397 +/- 65.263
1365	3140 P1-P1	-13.053 +/- 13.054	-60.367 +/- 62.241
	11736 P2-P2	-14.428 +/- 14.432	-63.388 +/- 65.256
	25792 P3-P3	-14.444 +/- 14.446	-63.432 +/- 65.287
5143	11084 P1-P1	-14.082 +/- 14.084	-62.656 +/- 64.495
	42736 P2-P2	-14.444 +/- 14.447	-63.435 +/- 65.288
	94960 P3-P3	-14.449 +/- 14.452	-63.449 +/- 65.296
Reference		-14.305 +- -14.305	-63.607 +- 65.160
Error		%	%

$\Delta t = 0.005\ \ \theta = 0.5$			
nel	ndof	ux of A [x 10^3]	uy of A [x 10^3]
319	832 P1-P1	-10.846 +/- 10.848	-56.049 +/- 56.053
	2936 P2-P2	-14.390 +/- 14.391	-63.738 +/- 64.703
	6316 P3-P3	-14.429 +/- 14.430	-63.833 +/- 64.810
1365	3140 P1-P1	-13.057 +/- 13.057	-60.813 +/- 61.826
	11736 P2-P2	-14.426 +/- 14.427	-63.827 +/- 64.801
	25792 P3-P3	-14.440 +/- 14.441	-63.854 +/- 64.845
5143	11084 P1-P1	-14.091 +/- 14.091	-63.195 +/- 63.981
	42736 P2-P2	-14.441 +/- 14.441	-63.856 +/- 64.847
	94960 P3-P3	-14.446 +/- 14.446	-63.865 +/- 64.860
Reference		-14.305 +- -14.305	-63.607 +- 65.160
Error		%	%

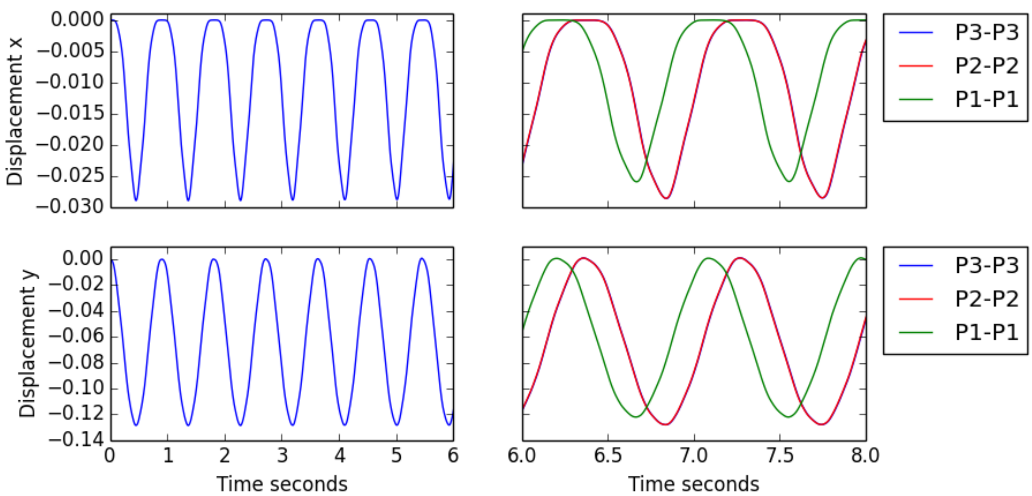

Figure 1.4: CSM-3, deformation components of A(t) for two different time intervals. Time interval $t \in [0, 6]$ shows the P3-P3 element pair, while$t \in [6, 8]$ compares all finite elemet pair chosen for the experiment

table 1.4, the displacement components of P3-P3 and P2-P2 elements can hardly be distinguished.

1.2.3 Validation of fluid structure interaction solver

The validation of the FSI solver constist of three sub-cases which will be referred to FSI-1, FSI-2 and FSI-3. The FSI-1 environment yields a steady state solution for the system, inducing small deformations to the elastic flag. This environment is excellent to ensure the overall coupling of the FSI-problem is executed properly. The FSI-2 and FSI-3 environment results in a periodic solution, where the elastic flag oscilates behind the sylinder.
For all sub-cases a parabolic velocity profile on the form,

$$v_f(0, y) = 1.5U \frac{(H - y)y}{(\frac{H}{2})^2}$$

is set on the left channel inflow. H is the height of the channel, while the parameter U is set differently to each problem to induce different flow profiles. At the right channel outflow, the pressure is set to $p = 0$. No-slip boundary conditions for the fluid are enforced on the channel walls, and on the circle of the inner geometry. The structure deformation and velocity is set to zero on the left side of the flag, where the flag is ancored to the circle. On the fluid-structure interface Γ, we enfore the kinematic and dynamic boundary condition

$$\mathbf{v}_f = \mathbf{v}_s \tag{1.1}$$

$$\sigma_f \cdot \mathbf{n} = \sigma_s \cdot \mathbf{n} \tag{1.2}$$

From chapter ?, (1.1) is enforced strongly due to the continious velocity field, while (1.2) is enforced weakly by omtitting form the weak formulation by.
Apart from the accuracy of the reported values, the main purpose of the validation of the fluid solver is twofold. Firstly, it is of great importance to ensure that the overall coupling of the fluid-structure interaction problem are executed correctly. Second, a good choice of mesh extrapolation model is essential to ensure that mesh entanglement is not present. Based on the experience with the previous sub-problems, the finite element group of P2-P2-P1 is chosen for deformation, velocity and pressure .

Table 1.9: Benchmark environment

Solid parameters			
parameter	FSI1	FSI2	FSI3
$\rho^s[10^3 \frac{kg}{m^3}]$	1	10	1
ν^s	0.4	0.4	0.4
$\mu^s[10^6 \frac{kg}{ms^2}]$	0.5	0.5	2.0
Fluid parameters			
$\rho^f[10^3 \frac{kg}{m^3}]$	1	1	1
$\nu^f[10^{-3} \frac{m^2}{s}]$	1	1	1
U	0.2	1	2
parameter	FSI1	FSI2	FSI3
Re	20	100	200

FSI1

Table 1.10: FSI 1 Results

Laplace					
nel	ndof	ux of A [x 10^3]	uy of A [x 10^3]	Drag	Lift
2474	21249	0.0226	0.8200	14.061	0.7542
7307	63365	0.0227	0.7760	14.111	0.7517
11556	99810	0.0226	0.8220	14.201	0.7609
Reference		0.0227	0.8209	14.295	0.7638
Linear Elastic					
nel	ndof	ux of A [x 10^3]	uy of A [x 10^3]	Drag	Lift
2474	21249	0.0226	0.8198	14.061	0.7541
7307	63365	0.0227	0.7762	14.111	0.751
11556	99810	0.0226	0.8222	14.201	0.7609
Reference		0.0227	0.8209	14.295	0.7638
Biharmonic bc1					
nel	ndof	ux of A [x 10^3]	uy of A [x 10^3]	Drag	Lift
2474	21249	0.0226	0.8200	14.061	0.7541
7307	63365	0.0227	0.7761	14.111	0.7517
11556	99810	0.0227	0.8017	14.205	0.9248
Reference		0.0227	0.8209	14.295	0.7638
Biharmonic bc2					
nel	ndof	ux of A [x 10^3]	uy of A [x 10^3]	Drag	Lift
2474	21249	0.0226	0.8200	14.061	0.7543
7307	63365	0.0227	0.7761	14.111	0.7518
11556	99810	0.0227	0.8020	14.205	0.9249
Reference		0.0227	0.8209	14.295	0.7638

Table 1.11: FSI 1 - No extrapolation

No extrapolation					
nel	ndof	ux of A [x 10^3]	uy of A [x 10^3]	Drag	Lift
2474	21249	0.0224	0.9008	14.064	0.7713
7307	63365	0.0226	0.8221	14.117	0.7660
11556	99810	0.0225	0.8787	14.212	0.7837
REF	REF	0.0227	0.8209	14.295	0.7638

FSI2

FSI2

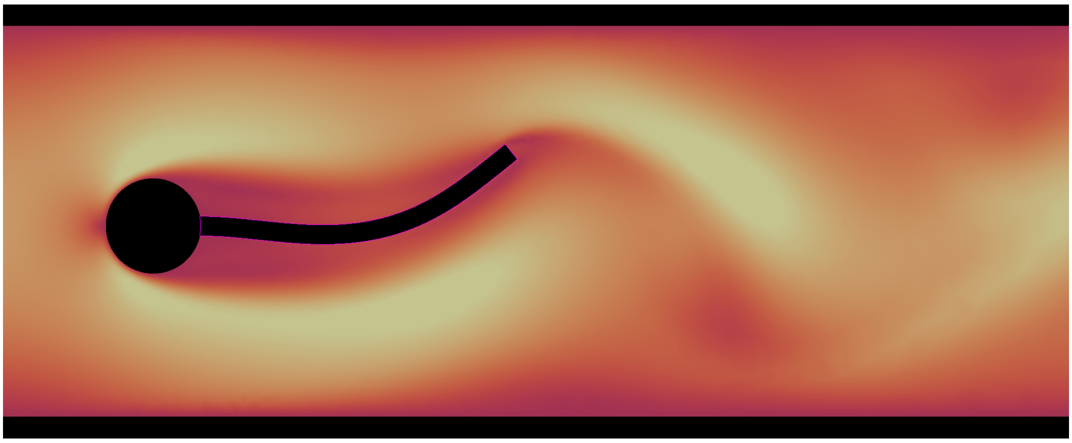

Figure 1.5: FSI-2, visualization of fully developed flow with structure deformation at time t = 9s

FSI3

Table 1.12: FSI 3 - Comparison of mesh extrapolation models

Laplace $\Delta t = 0.01 \theta = 0.51$					
nel	ndof	ux of A [x 10^3]	uy of A [x 10^3]	Drag	Lift
2474	21249	-2.41 ± 2.41	1.49 ± 3.22	449.40 ± 14.70	0.55 ± 155.80
7307	63365	-2.32 ± 2.30	1.34 ± 3.17	451.78 ± 16.08	1.13 ± 151.22
11556	99810	-2.34 ± 2.34	1.57 ± 3.19	455.92 ± 17.32	-0.10 ± 151.03
$\Delta t = 0.001 \theta = 0.501$					
nel	ndof	ux of A [x 10^3]	uy of A [x 10^3]	Drag	Lift
1216	5797	–2.17± 2.08	3.32 ± 29.07	439.98 ± 14.08	1.91 ± 151.71
2295	10730	-3.04 ± 2.88	1.51 ± 35.88	452.04 ± 22.41	3.30 ± 160.11
5963	27486	-3.03± 2.85	1.23 ± 35.97	459.45 ± 23.80	1.53 ± 160.14
Reference		136.7	10.53		
Error		0.007 %	0.001 %		

Biharmonic 1 $\Delta t = 0.01 \theta = 0.51$					
nel	ndof	ux of A [x 10^3]	uy of A [x 10^3]	Drag	Lift
2474	21249	7.96 ± 8.10	-3.84 ± 1.02	450.16 ± 15.11	-20.09 ± 148.17
7307	63365	3.10 ± 3.06	-1.90 ± 4.21	457.37 ± 15.24	-51.77 ± 127.28
11556	99810	-2.18 ± 9.65	1.31 ± 4.93	456.40 ± 17.45	0.45 ± 149.68
$\Delta t = 0.001 \theta = 0.5$					
nel	ndof	ux of A [x 10^3]	uy of A [x 10^3]	Drag	Lift
1216	5797	-2.18 ± 2.10	3.56 ± 2.90	435.19 ± 9.77	-1.57 ± 151.43
7307	63365	-1.42 ± 4.70	7.77 ± 2.85	454.38 ± 19.75	17.97 ± 155.08
11556	99810	-2.23 ± 6.16	1.72 ± 4.48	459.12 ± 22.97	-3.12 ± 171.22
Reference		-2.69 ± 2.56	1.48 ± 34.38	457.3 ± 22.66	2.22 ±- 149.78
Error		0.007 %	0.001 %		

Biharmonic 2 $\Delta t = 0.01 \theta = 0.51$					
nel	ndof	ux of A [x 10^3]	uy of A [x 10^3]	Drag	Lift
1216	5797	-1.74 ± 1.76	3.56 ± 26.01	439.41± 12.21	-1.35 ± 138.74
2295	10730	-2.39 ± 2.40	1.76 ± 32.27	449.71± 18.16	3.71 ± 149.97
$\Delta t = 0.001 \theta = 0.501$					
nel	ndof	ux of A [x 10^3]	uy of A [x 10^3]	Drag	Lift
1216	5797	-3.39 ± 3.38	1.23 ± 36.61	413.26 ± 51.82	57.19 ± 222.65
2295	10730	-4.70 ± 4.71	1.49 ± 44.62	427.91± 93.17	44.38 ± 268.05
Reference		-2.69 ± 2.56	1.48 ± 34.38	457.3 ± 22.66	2.22 ±- 149.78
Error		0.007 %	0.001 %		

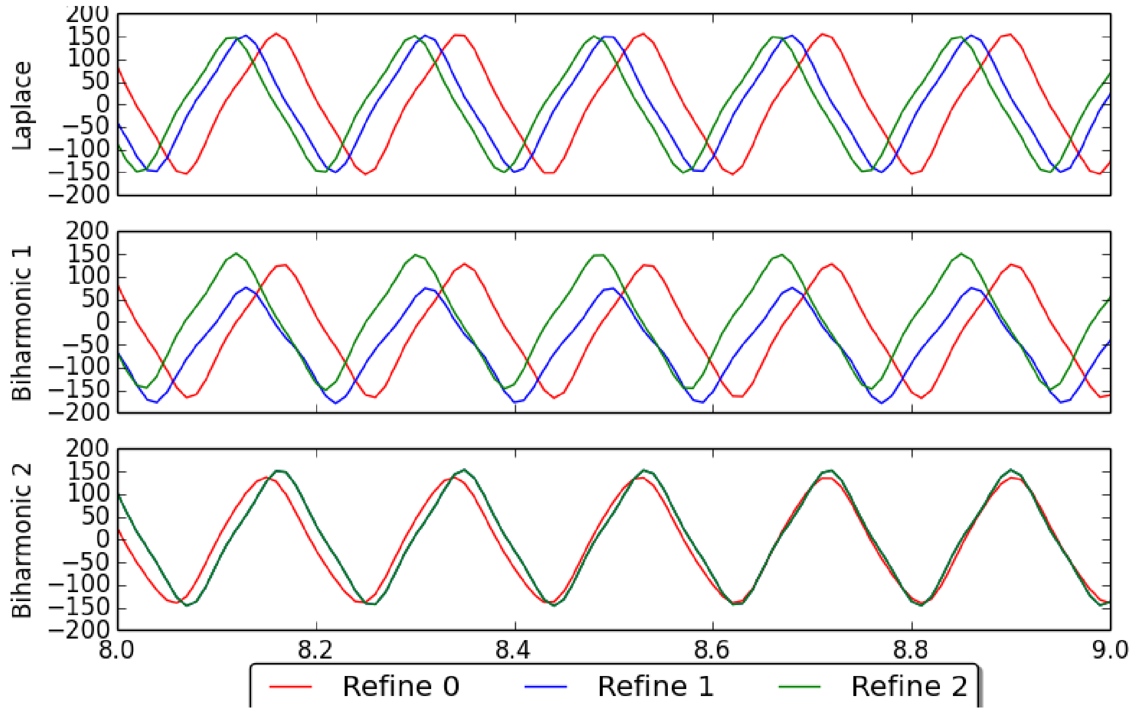

Figure 1.6: Comparing mesh extrapolation models

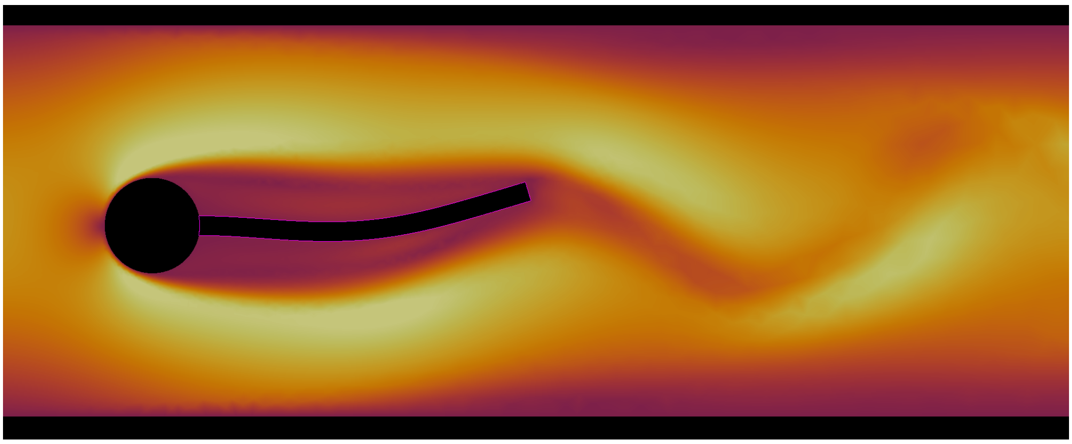

Figure 1.7: FSI-3, visualization of fully developped flow with structure deformation at time t = 5.1s

Discussion of results

Considering FSI1, all mesh extraplation models are of high accuracy compared to the reference solution. However, due to the small deformations of order 10^{-6}, FSI1 doesn't provide a rigorous test for testing mesh extrapolation models. By omitting mesh extrapolation from the variatonal formulation, reasonable results are still obtained. Therefore, the FSI-1 validation case can be misguiding, in terms of validating the chosen mesh extrapolation model.

The FSI2 case proved to be one of the most demanding tests, due to the large deformation of the elastic flag. leading to the risk of entangled mesh cells. Therefore

a high quality extrapolation of the solid deformation into the fluid is needed. All mesh extrapolation models proved to
The FSI3 environment does not induce deformation to the extent of the FSI2. However a critical phase in the transition to the periodic solution was discovered, where the pressure oscillation induces a large deformation to the system.

Bibliography

[1] Robert T Biedron and Elizabeth M Lee-Rausch. Rotor Airloads Prediction Using Unstructured Meshes and Loose CFD/CSD Coupling.

[2] P I Crumpton. Implicit time accurate solutions on unstructured dynamic grids. (95):1–23, 1995.

[3] J Donea, A Huerta, J.-Ph Ponthot, and A Rodríguez-Ferran. Arbitrary Lagrangian-Eulerian methods. (1969):1–38, 2004.

[4] Richard P Dwight. Robust Mesh Deformation using the Linear Elasticity Equations.

[5] Stéphane Étienne, D Tremblay, and Dominique Pelletier. Code Verification and the Method of Manufactured Solutions for Fluid-Structure Interaction Problems. *36th AIAA Fluid Dynamics Conference and Exhibit*, (June):1–11, 2006.

[6] Miguel A Fernández and Jean-Frédéric Gerbeau. Algorithms for fluid-structure interaction problems. 2009.

[7] Miguel A. Fernández, Jean Frederic Gerbeau, and Ceremade Grandmont. A projection semi-implicit scheme for the coupling of an elastic structure with an incompressible fluid. *International Journal for Numerical Methods in Engineering*, 69(4):794–821, 2007.

[8] L Formaggia and F Nobile. A stability analysis for the arbitrary Lagrangian Eulerian formulation with finite elements. *East-west journal of numerical mathematics*, Vol. 7(No. 2):105–131, 1991.

[9] Luca Formaggia and Fabio Nobile. Stability analysis of second-order time accurate schemes for ALE-FEM. *Computer Methods in Applied Mechanics and Engineering*, 193(39-41 SPEC. ISS.):4097–4116, 2004.

[10] Christiane Förster, Wolfgang A. Wall, and Ekkehard Ramm. Artificial added mass instabilities in sequential staggered coupling of nonlinear structures and incompressible viscous flows. *Computer Methods in Applied Mechanics and Engineering*, 196(7):1278–1293, 2007.

[11] Bernhard Gatzhammer. Efficient and Flexible Partitioned Simulation of Fluid-Structure Interactions. page 261, 2014.

[12] Philippe Geuzaine. Numerical Simulations of Fluid-Structure Interaction Problems using MpCCI. (1):1–5.

[13] Brian T. Helenbrook. Mesh deformation using the biharmonic operator. *International Journal for Numerical Methods in Engineering*, 2003.

[14] Gerhard A. Holzapfel. *Nonlinear Solid Mechanics: A Continuum Approach for Engineering.* 2000.

[15] Jaroslav Hron and Stefan Turek. Proposal for numerical benchmarking of fluid-structure interaction between an elastic object and laminar incompressible flow. *Fluid-Structure Interaction*, 53:371–385, 2006.

[16] Ming-Chen Hsu and Yuri Bazilevs. Fluid–structure interaction modeling of wind turbines: simulating the full machine. *Computational Mechanics*, 50(6):821–833, dec 2012.

[17] Su-Yuen Hsu, Chau-Lyan Chang, and Jamshid Samareh. A Simplified Mesh Deformation Method Using Commercial Structural Analysis Software.

[18] Hrvoje Jasak and Željko Tuković. Automatic mesh motion for the unstructured Finite Volume Method. *Transactions of Famena*, 30(2):1–20, 2006.

[19] Jae-Hyun Kim and Hyung-Cheol Shin. Application of the ALE technique for underwater explosion analysis of a submarine liquefied oxygen tank. *Ocean Engineering*, 35(8-9):812–822, jun 2008.

[20] V V Meleshko. Bending of an Elastic Rectangular Clamped Plate: Exact Versus 'Engineering' Solutions. *Journal of Elasticity*, 48(1):1–50, 1997.

[21] José Merodio and Giuseppe Saccomandi. Continuum Mechanics - Volume I. In *Volume 1*, chapter 3, pages 82–84. EOLSS, 2011.

[22] Selim MM and Koomullil RP. Mesh Deformation Approaches – A Survey. *Journal of Physical Mathematics*, 7(2), 2016.

[23] J Newman. *Marine Hydrodynamics.* 1977.

[24] William L. Oberkampf and Christopher J. Roy. *Verification and Validation in Scientific Computing.* Cambridge University Press, Cambridge, 2010.

[25] M Razzaq, Stefan Turek, Jaroslav Hron, J F Acker, F Weichert, I Grunwald, C Roth, M Wagner, and B Romeike. Numerical simulation and benchmarking of fluid-structure interaction with application to Hemodynamics. *Fundamental Trends in Fluid-Structure Interaction*, 1:171–199, 2010.

[26] T. Richter and T. Wick. Finite elements for fluid-structure interaction in ALE and fully Eulerian coordinates. *Computer Methods in Applied Mechanics and Engineering*, 199(41-44):2633–2642, 2010.

[27] Thomas Richter. Fluid Structure Interactions. 2016.

[28] Thomas Richter and Thomas Wick. On Time Discretizations of Fluid-Structure Interactions. pages 377–400. 2015.

[29] Patrick J. Roache. Code Verification by the Method of Manufactured Solutions. *Journal of Fluids Engineering*, 124(1):4, 2002.

[30] P.J. Roache. *Verification and Validation in Computational Science and Engineering*. Computing in Science Engineering, Hermosa Publishers, 1998, 8-9, 1998.

[31] Edward J. Rykiel. Testing ecological models: The meaning of validation. *Ecological Modelling*, 90(3):229–244, 1996.

[32] Kambiz Salari and Patrick Knupp. Code Verification by the Method of Manufactured Solution. Technical report, Sandia National Laboratories, 2000.

[33] LE Schwer. Guide for verification and validation in computational solid mechanics. *American Society of Mechanical Engineers*, PTC 60(V&V 10):1–15, 2006.

[34] Jason P Sheldon, Scott T Miller, and Jonathan S Pitt. Methodology for Comparing Coupling Algorithms for Fluid-Structure Interaction Problems. *World Journal of Mechanics*, 4(February):54–70, 2014.

[35] J.C. Simo and F. Armero. Unconditional stability and long-term behavior of transient algorithms for the incompressible Navier-Stokes and Euler equations. *Computer Methods in Applied Mechanics and Engineering*, 111(1-2):111–154, jan 1994.

[36] Ian Sommerville. Verification and Validation. Technical Report February, 2006.

[37] K Stein, T Tezduyar, and R Benney. Mesh Moving Techniques for Fluid-Structure Interactions With Large Displacements.

[38] Keith Stein, Richard Benney, Tayfun Tezduyar, and Jean Potvin. Fluid–structure interactions of a cross parachute: numerical simulation. *Computer Methods in Applied Mechanics and Engineering*, 191(6-7):673–687, dec 2001.

[39] Ryo Torii, Marie Oshima, Toshio Kobayashi, Kiyoshi Takagi, and Tayfun E. Tezduyar. Fluid–structure interaction modeling of a patient-specific cerebral aneurysm: influence of structural modeling. *Computational Mechanics*, 43(1):151–159, dec 2008.

[40] A V, T Passerini, A Quaini, U Villa, A Veneziani, and S Canic. Numerical Analysis and S cientific C omputing P reprint S eria Validation of an open source framework for the simulation of blood flow in rigid and deformable vessels P reprint # 17 D epartment of Mathematics University of Houston. 2013.

[41] Jan Vierendeels. Comparison of the Hemodynamic and Thrombogenic Performance of Two Bileaflet Mechanical Heart Valves Using a CFD/FSI Model. *Journal of Biomechanical Engineering*, 129(4):558, jan 2007.

[42] Wolfgang A. Wall, Axel , Gerstenberger, Peter , Gamnitzer, Christiane , Förster, and Ekkehard , Ramm. Large Deformation Fluid-Structure Interaction – Advances in ALE Methods and New Fixed Grid Approaches. In *Fluid-Structure Interaction: Modelling, Simulation, Optimisation*, pages 195—-232. Springer Berlin Heidelberg, 2006.

[43] Frank White. *Viscous fluid flow.* McGraw-Hill, third edit edition.

[44] T. Wick. Stability Estimates and Numerical Comparison of Second Order Time-Stepping Schemes for Fluid-Structure Interactions. In *Numerical Mathematics and Advanced Applications 2011*, pages 625–632. Springer Berlin Heidelberg, Berlin, Heidelberg, 2013.

[45] T Wick and Thomas Wick. Variational-monolithic ALE fluid-structure interaction: Comparison of computational cost and mesh regularity using different mesh motion techniques.

[46] Thomas Wick. *Adaptive Finite Element Simulation of Fluid-Structure Interaction with Application to Heart-Valve.* PhD thesis, Heidelberg.

[47] Thomas Wick. Solving Monolithic Fluid-Structure Interaction Problems in Arbitrary Lagrangian Eulerian Coordinates with the deal.II Library.

[48] Thomas Wick. Fluid-structure interactions using different mesh motion techniques. *Computers and Structures*, 89(13-14):1456–1467, 2011.

[49] Thomas Wick. Fully Eulerian fluid-structure interaction for time-dependent problems. *Computer Methods in Applied Mechanics and Engineering*, 255:14–26, 2013.

[50] Klaus Wolf, Schloss Birlinghoven, Code Coupling Interface, Open Programming Interface, and Distributed Simulation. Mpcci – the Generl Code Coupling Interface. *6. LS-DYNA Anwenderforum, Frankenthal 2007 IT*, pages 1–8, 2007.

[51] P. Wriggers. *Computational contact mechanics, second ed., Springer*. 2006.

[52] Hou Zhang, Xiaoli Zhang, Shanhong Ji, Yanhu Guo, Gustavo Ledezma, Nagi Elabbasi, and Hugues DeCougny. Recent development of fluid-structure interaction capabilities in the ADINA system. *Computers and Structures*, 81(8-11):1071–1085, 2003.